Dynamic Modelling of *Haematococcus pluvialis* Photoinduction for Astaxanthin Production in both Attached and Suspended Photobioreactors

Dongda Zhang[a,ǂ,*], Minxi Wan[b,ǂ], Ehecatl A. del Rio-Chanona[a], Jianke Huang[b], Weiliang Wang[b], Yuanguang Li[b], Vassilios S. Vassiliadis[a,*]

a: Department of Chemical Engineering and Biotechnology. University of Cambridge, Pembroke Street. Cambridge CB2 3RA, UK.

b: State Key laboratory of Bioreactor Engineering, East China University of Science and Technology, Shanghai 200237, PR China.

ǂ: These authors contributed equally to this work.

*: corresponding author, email: dz268@cam.ac.uk (Dongda Zhang), tel: 44 (0)1223 330132; email: vsv20@cam.ac.uk (Vassilios S. Vassiliadis), tel: 44 (0)1223 330142.

Abstract

Haematococcus pluvialis is a green algae with the great potential to generate natural astaxanthin. In the current study, dynamic models have been proposed to simulate effects of light intensity, light attenuation, temperature and nitrogen quota on cell growth and astaxanthin production in both suspended and attached photobioreactors, which to the best of our knowledge has not been addressed before. Based on the current models, optimal temperatures for algal growth and astaxanthin accumulation are identified. Cell absorption is found to be the primary factor causing light attenuation in the suspended reactor. In this reactor, astaxanthin accumulation is limited by the low local light intensity due to light attenuation during the initial operation period, but almost independent from that once it is close to the maximum value. Compared to the suspended reactor, light attenuation in the attached reactor is much reduced and biomass growth is remarkably enhanced, which suggests the attached reactor is a better choice if the process aims for biomass cultivation. However, the well-mixed culture in the suspended reactor can push most cells toward astaxanthin production; while the attached reactor has the potential to prevent the accumulation of astaxanthin in the bottom algae. Therefore, the suspended photobioreactor should be selected if the process target is astaxanthin production.

Keywords: astaxanthin; dynamic simulation; light attenuation; temperature; suspended photobioreactor; attached photobioreactor.

1. Introduction

Astaxanthin (3,3'-dihydroxy-β, β-carotene-4,4'-dione) is a high-value carotenoid pigment with wide applications in the cosmetic, pharmaceutical, and food industries [1], [2]. It is considered as a promising bioproduct for future commercialisation due to its high antioxidant activity and significant impact on animal pigmentation [3]. Although synthetic astaxanthin dominates the current commercial market and has achieved a profit of $200M per year, the huge demand of natural astaxanthin is still an open challenge at present [4]. To fill the gap, green alga *Haematococcus pluvialis* has been chosen as the best candidate for astaxanthin production because of its high astaxanthin content (up to 5%), and several companies have been set up to produce natural astaxanthin from this species [5], [6].

Extensive research has been conducted to determine the optimal operating conditions for astaxanthin production. High irradiance, high temperature, oxidative stress, and nitrogen-deprivation have been found to significantly stimulate the accumulation of astaxanthin, while these operating conditions are not favourable for *H. pluvialis* growth [2], [7]–[10]. To enhance the productivity of astaxanthin, a two-stage cultivation method is widely used. The first stage aims to cultivate algae in conditions where cells grow fast and remain green with the presence of a nitrogen source in the culture; in the second stage (induction stage), cells are subjected to a nitrogen-deprived culture for the induction of astaxanthin. Because of the accumulation of astaxanthin, cells in the second stage usually turn to be red [1], [2], [11].

Although there are extensive laboratory measurements for the system, much less effort has been focused on the modelling of these stages. Dynamic simulation is an effective tool to determine the optimal operating conditions for both laboratory scale and industrial scale astaxanthin production processes. In particular, the induction stage where cells stop growing and astaxanthin commences to accumulate is very difficult to model due to the complicated metabolic mechanisms involved. Although a few researchers constructed dynamic models to simulate this process [1], [12]–[16], these models have severe limitations which restrict their applicability.

First, as the experiments in these publications show a very distinct astaxanthin accumulation tendency led by the different operating conditions [12], [14], [16], these models can only be used to simulate specific processes whose operating conditions are similar. Second, these models only consider the effect of one factor (light intensity or nutrient concentration) on cell growth and astaxanthin production, but do not include other factors such as temperature and intracellular nutrient concentration [1], [13], [14]. Furthermore, none of these works [1], [12]–[16] decouple the two cultivation stages into separate models, although the operating conditions and performance of these stages are quite different. For this, it is reasonable to consider that these models may not simulate the induction stage with a high accuracy.

Therefore, to simulate accurately the dynamic process of the induction stage, the current study aims to construct rigorous models including the effects of temperature, light intensity, light attenuation and nitrogen-deficiency on algal growth and astaxanthin accumulation,

which to the best of our knowledge has not been explored. Different reactor types, including both suspended reactor and attached reactor are considered in the current work. The complex relation between astaxanthin accumulation and algal growth has also been comprehensively summarised in this work and will be introduced in next section.

2. Experiment setup and Model Construction

2.1 Experiments setup

Two types of photobioreactor (PBR), the suspended PBR (shown in Figure 1(a)) and the attached PBR (shown in Figure 1(b)), have been chosen to process the induction stage in our previous experimental work [4], [11]. The suspended PBR is a 1 L column reactor with height of 26 cm and diameter of 7 cm. Light is provided from one side of the reactor. For the attached reactor, a microfiltration membrane (diameter of 33 ± 0.5 cm) was used to form an algal film and then placed onto a gauze which was vertically located in a medium reservoir. Illumination is also provided from one side of the reactor.

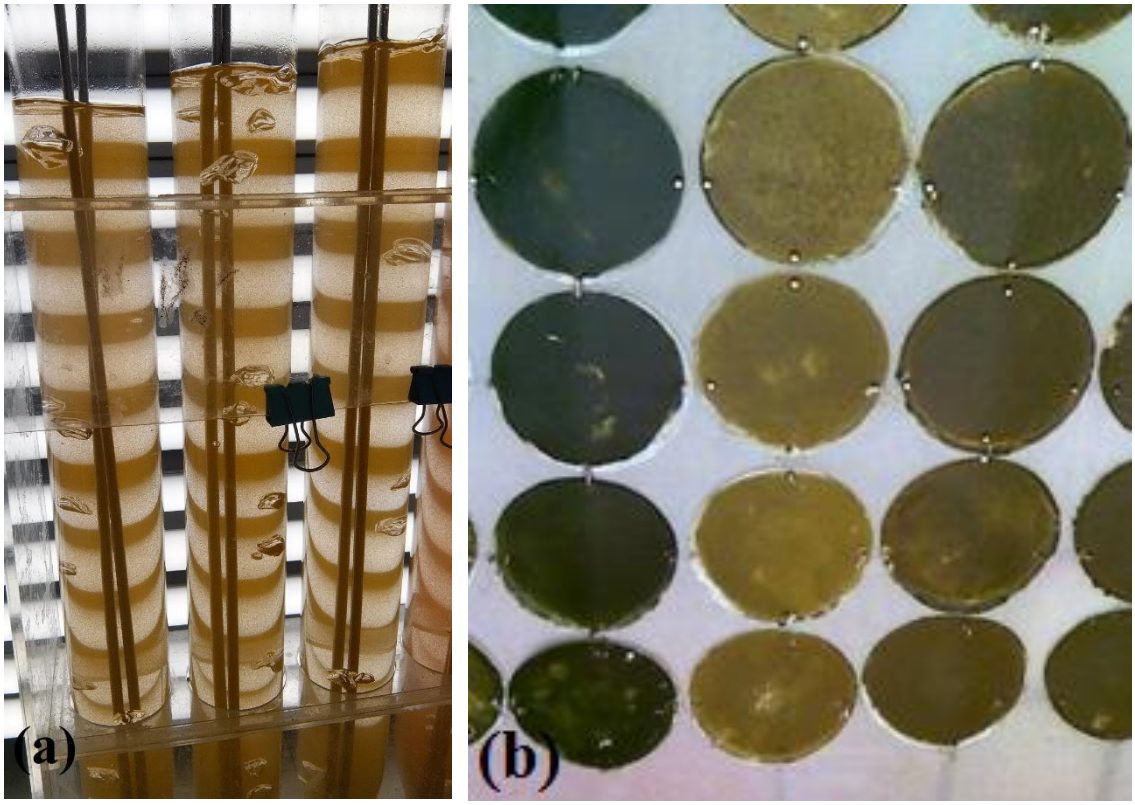

Figure 1: Photobioreactors used in the current study. (a) suspended PBR; (b) attached PBR.

The current work aims to contribute rigorous models capable of accurately simulating the different cell growth and astaxanthin accumulation trends presented in both previous publications and current experiments. As a potential reason why there are quite different experimental observations between these works is attributed to the selection of different *H. pluvialis* strains [4], [12], [14], in the current study two different *H. pluvialis* strains, *H. pluvialis* NIES-144 and *H. pluvialis* ZY-18, are used in our experimental research and cultivated in different operating conditions for model construction.

H. pluvialis NIES-144 was used to test the effect of initial biomass concentration on cell growth and astaxanthin production in both suspended reactor and attached reactor. Incident

light intensity and temperature in these experiments were fixed at 150 μmol·m^{-2}·s^{-1} and 25℃, respectively. *H. pluvialis* ZY-18 was mainly used to test the effect of temperature on algal growth and astaxanthin accumulation. Incident light intensity in these experiments was fixed at 250 μmol·m^{-2}·s^{-1}. In order to demonstrate the predictability of the current models, two additional experiments were carried out under different operating conditions, and will be introduced in Section 3.3. All of the experiments were replicated three times. Details of experiment design and information of strains can be found in our previously published studies [4], [11].

2.2 Model construction

Two dynamic models, Model 1 and Model 2, have been proposed in the current study and are presented through Equations (1)-(3) and Equations (4)-(6), respectively. The two models are constructed based on different kinetic mechanism assumptions. Both of the models are used to simulate biomass growth and astaxanthin accumulation in both the attached PBR and the suspended PBR. To guarantee a dynamic model capable of accurately simulating both algal growth and astaxanthin production under different operating conditions, the following characteristics were integrated:

1. The accumulation of astaxanthin and the growth of biomass are dependent on the intracellular nitrogen quota;
2. Biomass growth rate may increase rapidly at the beginning and then slow down;
3. Biomass decay can be found after cells stop growing;
4. Astaxanthin accumulation rate increases initially and then slows down;

5. A maximum astaxanthin content exists in cells;

6. It is not necessary for the astaxanthin accumulation rate to have the same tendency as that of the biomass growth rate, which means astaxanthin can stop accumulating either much earlier or much later than the termination of biomass growth;

7. A slight decrease of astaxanthin content can be observed after the accumulation of astaxanthin;

8. Both astaxanthin accumulation rate and biomass growth rate are dependent on the culture temperature and light intensity.

All of these characteristics are summarised from previous publications and will be introduced in detail in later sections. Both models are derived from the Droop model and the Luedeking-Piret model [17], [18].

Dynamic model 1:

$$\frac{dX}{dt} = \left(1 - \frac{k_q}{q}\right) \cdot \frac{I}{I + k_s} \cdot \left[A \cdot \mathrm{e}^{-\frac{E_a}{R \cdot T}} - B \cdot \mathrm{e}^{-\frac{E_b}{R \cdot T}}\right] \cdot X - \mu_d \cdot X^2 \quad (1)$$

$$\frac{dq}{dt} = -\left(1 - \frac{k_q}{q}\right) \cdot \frac{I}{I + k_s} \cdot \left[A \cdot \mathrm{e}^{-\frac{E_a}{R \cdot T}} - B \cdot \mathrm{e}^{-\frac{E_b}{R \cdot T}}\right] \cdot q \quad (2)$$

$$\frac{dw}{dt} = \left[b + \left(1 - \frac{k_{qw}}{q}\right)\right] \cdot \frac{k_{qw}}{q} \cdot \left(1 - \frac{w}{w_{\max}}\right) \cdot \frac{I}{I + k_{sw}} \cdot \left[A_w \cdot \mathrm{e}^{-\frac{E_{aw}}{R \cdot T}} - B_w \cdot \mathrm{e}^{-\frac{E_{bw}}{R \cdot T}}\right] \quad (3)$$

Dynamic model 2:

$$\frac{dX}{dt} = \left(1 - \frac{k_q}{q}\right) \cdot \frac{k_q}{q} \cdot \frac{I}{I + k_s} \cdot \left[A \cdot \mathrm{e}^{-\frac{E_a}{R \cdot T}} - B \cdot \mathrm{e}^{-\frac{E_b}{R \cdot T}}\right] \cdot X - \mu_d \cdot X^2 \quad (4)$$

$$\frac{dq}{dt} = -\left(1 - \frac{k_q}{q}\right) \cdot \frac{I}{I + k_s} \cdot \left[A \cdot \mathrm{e}^{-\frac{E_a}{R \cdot T}} - B \cdot \mathrm{e}^{-\frac{E_b}{R \cdot T}}\right] \cdot k_q \quad (5)$$

$$\frac{dw}{dt} = \left[b + \left(1 - \frac{k_{qw}}{q}\right)\right] \cdot \frac{k_{qw}}{q} \cdot \left(1 - \frac{w}{w_{\max}}\right) \cdot \frac{I}{I + k_{sw}} \cdot \left[A_w \cdot \mathrm{e}^{-\frac{E_{aw}}{R \cdot T}} - B_w \cdot \mathrm{e}^{-\frac{E_{bw}}{R \cdot T}}\right] \quad (6)$$

where X is biomass concentration; q is normalised nitrogen quota; k_q and k_{qw} are

normalised minimum nitrogen quota for cell growth and astaxanthin production, respectively; I is local light intensity; k_s and k_{sw} are light saturation terms for cell growth and astaxanthin production, respectively; A and B are pre-exponential coefficients; E_a and $E_{a,w}$ are activation energy for cell growth and astaxanthin accumulation, respectively; w is astaxanthin content; $w_{\max}$ is maximum astaxanthin content; μ_d is cell decay rate; b is growth non-associated coefficient for astaxanthin production.

2.2.1 Nitrogen quota (intracellular nitrogen concentration)

In this section, characteristics 1--7 from the above itemised list, and the design of both models will be explained in detail. The nitrogen quota is the ratio of intracellular nitrogen element weight to dry cell weight, which is used to represent the intracellular nitrogen concentration in cells. As the culture in the current study is nitrogen-free, nitrogen quota in cells is lower than that in a nitrogen-sufficient culture. Since the nitrogen quota was not measured in the present study, a normalised nitrogen quota is used to replace the absolute value of nitrogen quota and is defined as the ratio of nitrogen quota between the current culture and the nitrogen-sufficient culture [17].

In a nitrogen-deprived culture, the photosynthetic electron transport chain in *H. pluvialis* is heavily damaged due to the significant reduction of cytochrome b_6/f complex. In order to prevent cells being over-reduced by photosynthesis, the astaxanthin sysnthesis and plastid terminal oxidase-mediated electron transport pathways are stimulated, with the activities of these pathways being enhanced by the extent of cell nitrogen-deficiency [19], [20].

174 Meanwhile, due to the decreased activity of the starch generation pathway, cell growth rate is
175 also affected [21]. As the transcription of essential enzymes involved in these processes
176 requires the participation of nitrogen, both astaxanthin accumulation and cell growth will
177 eventually cease once the intracellular nitrogen concentration drops to its minimum value
178 (characteristics 1 and 4).
179
180 For biomass growth rate, the effect of the nitrogen quota is more complicated. Although most
181 of previous work found that biomass growth rate generally decreases with the decreasing
182 nitrogen quota in suspended PBRs [3], [11], [22], [23] have shown recently that *H. pluvialis*
183 growth rate may increase in the initial cultivation period in an outdoor PBR. This
184 phenomenon, is apparently observed in our very recent work [4] where *H. pluvialis* was
185 cultivated in another reactor type, the attached PBR, and biomass growth rate is found to
186 continuously increase in a nitrogen-free culture for 12 days (characteristic 2).
187
188 To consider this fact, in the current work two different models are composed and will be
189 compared later. In Model 1 (Equation (1)), the term $\left(1-\frac{k_q}{q}\right)$ represents the decrease of
190 biomass growth rate due to the aggravated extent of nitrogen-deficiency. This equation
191 assumes that the increase of biomass growth rate is led by the increasing biomass
192 concentration (X), rather than the extent of nitrogen-deficiency. In Model 2 (Equation (4)),
193 the term $\frac{k_q}{q}$, whose value increases with the decreasing nitrogen quota (q), is embedded with
194 the assumption that the enhancement in biomass growth rate is also led by
195 nitrogen-deficiency. Furthermore, since biomass decay has been observed in previous

196 publications [7], [22]–[24], another term, $\mu_d \cdot X^2$, is added in both equations to take biomass
197 decay into account [17] (characteristic 3).
198
199 For astaxanthin, as its synthesis is enhanced by the extent of nitrogen-deficiency initially and
200 depressed after the nitrogen quota is significantly reduced, the accumulation rate increases
201 initially and then slows down in the process [3], [4], [23]. Therefore, in Equations (3) and (6)
202 the term $\frac{k_{qw}}{q}$ is used to represent the extent of nitrogen-deficiency, and the term $\left[b + \right.$
203 $\left.\left(1 - \frac{k_{qw}}{q}\right)\right]$ is used to represent the decrease of astaxanthin accumulation rate caused by
204 nitrogen-deficiency since this term decreases with the decreasing q. As a maximum
205 astaxanthin content has been observed in previous studies [11], [23], [25], in the current
206 models the term $\left(1 - \frac{w}{w_{\max}}\right)$ is included in Equations (3) and (6) to ensure the astaxanthin
207 content cannot exceed the maximum value (characteristic 5).
208
209 Finally, $\left[b + \left(1 - \frac{k_{qw}}{q}\right)\right]$ in Equations (3) and (6) is also used to simulate the fact that
210 astaxanthin accumulation rate does not necessarily show the same tendency with biomass
211 growth rate, as astaxanthin may stop accumulating either much earlier or much later than the
212 termination of biomass growth at different operating conditions [3], [4], [14]. In this term, b
213 represents the growth non-associated accumulation rate and $\left(1 - \frac{k_{qw}}{q}\right)$ represents the growth
214 associated accumulation rate. If astaxcanthin stops being generated before the termination of
215 cell growth, $k_{qw} > k_q$ and $b = 0$. If astaxanthin continues accumulating after the
216 termination of biomass growth, $b > 0$ and $k_{qw} < k_q$ (characteristic 6).
217

More specifically, this term is also capable of simulating the slight decrease of astaxanthin at the end of the process, as observed in recently published work[11], [23]. In this case, once q drops lower than k_{qw}, $\left(1-\frac{k_{qw}}{q}\right)$ will be negative and astaxanthin accumulation rate will be negative if b is lower than the absolute value of $\left(1-\frac{k_{qw}}{q}\right)$ (characteristic 7).

2.2.2 Light intensity

In Sections 2.2.2 and 2.2.3, characteristic 8 will be explained in detail.

2.2.2.1 Simulation of light intensity effects

Light intensity significantly affects both biomass growth and astaxanthin accumulation rates [1], [9]. In general, the effect of light intensity on cell growth can be described by the Aiba model as in Equation (7) [26]. In our experiments, as the incident light intensities in both suspended reactor and attached reactor are not higher than 250 μmol·m^{-2}·s^{-1} where photo-inhibition is not observed [4], the photo-inhibition term in the Aiba model is neglected.

$$\mu = \mu_{\max} \cdot \frac{I}{I + k_s + \frac{I^2}{k_i}} \tag{7}$$

$\mu_{\max}$ represents the maximum specific growth rate, I represents the light intensity, k_s represents the light saturation coefficient and k_i represents the photo-inhibition coefficient.

2.2.2.2 Light attenuation in suspended reactor

It is notable that the illumination cells experience in the reactor is not the same with the incident light intensity due to light attenuation. With the existence of light attenuation, local light distribution in a photobioreactor is in general non-uniform and much lower than incident

light intensity. In suspended reactors, recent research found that light attenuation is mainly caused by bubble reflection and microorganism absorption [27], [28]. Although in theory microorganism scattering can also contribute to light attenuation, its effect has been demonstrated to be negligible by previous research and thus not included in this study [29][27].

Extensive research has been conducted to explore light attenuation in flat plate PBRs [30]–[32], for which Equation (8) is mainly used to estimate the local light intensity [32]. For column PBRs, previous research also proposed some light transmission models [33], [34], with most being very complicated and making the dynamic model parameter estimation procedure difficult to carry out.

As the current model consists of highly non-linear differential equations, its parameter estimation has been demonstrated to be difficult, as advanced discretisation and optimisation methods have to applied and significant computational cost will be introduced [35], [36]. Therefore, in order to ensure the accurate calculation of the current parameter estimation procedure, Equation (8) is selected to reduce the current model complexity.

$$I = I_0 \cdot \mathrm{Exp}\left[-\left(\frac{3\alpha_g}{d_b} + \alpha \cdot X\right) \cdot z\right] \quad (8)$$

I is the local light intensity, I_0 is the incident light intensity, α_g is the bubble volume fraction, d_b is the bubble average diameter, α is the algal absorption coefficient, z is the distance the light travels through the reactor.

In the present research, a column PBR was selected in our experiments and illumination was only provided from one side of the 1 L reactor (height: 26 cm, diameter: 7 cm). Air was pumped into the suspended reactor for *H. pluvialis* photo-autotrophic growth, so that both bubble reflection and algal absorption have to be included. In order to estimate the local light intensity inside the reactor, some simplification was applied in the current study. In particular, as suggested by a recent publication [37], it is assumed that the current reactor is a flat plate PBR with a square bottom surface. The square area is the same with the circle area, which means the length of the square is 6.20 cm. As both bubble average diameter and bubble volume fraction are in general estimated based on computational fluid dynamics whilst these parameters are kept constant in the current experiment, $\frac{3\alpha_g}{d_b}$ in Equation (8) is replaced by k_l for the convenience of future parameter estimation procedure. Hence, Equation (8) can be re-written as Equation (9).

$$I = I_0 \cdot \mathrm{Exp}[-(k_l + \alpha \cdot X) \cdot z] \quad (9)$$

2.2.2.3 Light attenuation in attached reactor

For attached PBRs or biofilms, the study of light attenuation has received little attention. Although biomass generally only grows from hundreds of microns to several millimeters, severe light attenuation has been observed and reported in recent studies [38]–[40]. To include this factor in the present simulation it is assumed that algae only grow along the direction perpendicular to the reactor surface, towards the light source. Based on the current assumption, biomass density (ρ_X) on the cross section through the light transmission direction is constant, because cells predominantly grow along this way. As a result, the algal absorption

coefficient on each cross section is the same. Therefore, local light intensity in an attached reactor can be calculated by Eq. (10).

$$I = I_0 \cdot \mathrm{Exp}[-\beta' \cdot h] \quad (10)$$

where β' is algal absorption coefficient, h is biofilm thickness from the top (exposure) surface to the research surface.

The weight of biofilm (m) with a thickness of h is calculated as $m = h \cdot \rho_X \cdot S$, where S is the biofilm surface area. In general, biomass concentration (X) in attached reactors is represented by g·m^{-2} ($X = \frac{m}{S}$), therefore Equation (10) can be re-written as Equation (11) below.

$$I = I_0 \cdot \mathrm{Exp}[-\beta' \cdot h] = I_0 \cdot \mathrm{Exp}\left[-\beta' \cdot \frac{X}{\rho_X}\right] = I_0 \cdot \mathrm{Exp}[-\beta \cdot X] \quad (11)$$

where β is the biomass concentration based algal absorption coefficient.

2.2.2.4 Simplification of spatial dimension

The current models include both spatial variations due to light attenuation, and temporal variations as the processing considered is dynamic. To eliminate the spatial variation, two methods have been proposed recently. The first one is to replace local light intensities by an average light intensity which is calculated by Equation (12) in a suspended reactor, and by Equation (13) in an attached reactor. The second method is to use the average biomass growth rate, which turns out to be equivalent to calculation of the average value of ($\frac{I}{I+k_s}$) since it is the only spatially varying term. Equations (14) and (15) show the average value of this term in suspended reactors and attached reactors, respectively.

$$I_{ave} = I_0 \cdot \frac{1 - \mathrm{e}^{-(k_l + \alpha \cdot X) \cdot L}}{(k_l + \alpha \cdot X) \cdot L} \quad (12)$$

$$I_{ave} = I_0 \cdot \frac{1 - \mathrm{e}^{-\beta \cdot X \cdot L}}{\beta \cdot X \cdot L} \quad (13)$$

$$\left(\frac{I}{I + k_s}\right)_{ave} = \frac{\ln[I_0 + k_s] - \ln\left[I_0 \cdot \left(-L \cdot (k_l + \alpha \cdot X)\right) + k_s\right]}{L \cdot (k_l + \alpha \cdot X)} \quad (14)$$

$$\left(\frac{I}{I + k_s}\right)_{ave} = \frac{\ln[I_0 + k_s] - \ln[I_0 \cdot (-L \cdot \beta \cdot X) + k_s]}{L \cdot \beta \cdot X} \quad (15)$$

In most of the previous studies [1], [12], [41], the first method is widely selected simply due to its convenience for parameter estimation. Although some researchers recently used the second method and found that it shows high agreement with experimental results [10], [42], none of them compared the accuracy of the two methods. To explore which method is more accurate and suitable for further studies, both simplifications are selected and compared in the present study.

2.2.3 Temperature

Temperature is also found to influence remarkably the rate of cell growth, cell decay and bioproduct accumulation An optimal temperature exists to facilitate microbial biomass growth and bioproduct synthesis [9], [13]. The Arrhenius equation has been widely used to describe the effects of temperature on both biomass growth and bioproduct production [43]–[45], and is shown in Equation (16).

$$\mu = A \cdot \mathrm{e}^{-\frac{E_a}{R \cdot T}} - B \cdot \mathrm{e}^{-\frac{E_b}{R \cdot T}} \quad (16)$$

where E_A is the activation energy of cell growth or bioproduct production, E_B is the

inactivation energy of cell growth or bioproduct production, and A and B are pre-exponential factors.

As previous research [1], [3], [41] has demonstrated, the favourable range of temperature and light intensity for *H. pluvialis* growth and astaxanthin accumulation may be different, hence in our model construction parameters in both the Aiba model and Arrhenius equation for biomass growth and astaxanthin generation are not assumed necessarily to be the same.

2.3 Parameter estimation process

To estimate the parameters that best described the models presented in this work a nonlinear programming problem (NLP) was formulated. The original system was discretised through orthogonal collocation. Orthogonal collocation is a highly robust discretisation strategy, as it needs relatively few finite elements and is stable even when confronted with stiff systems [46], [47]. The computational implementation of this work was done in a Python-based optimisation environment [48]. IPOPT [49], an interior point optimiser, was used as a solver to find the optimal solution for the resulting NLP.

3 Results and discussion

3.1 Parameters in *H. pluvialis* ZY-18 models

For *H. pluvialis* ZY-18, only the suspended reactor was used in our experimental work. Table 1 shows the parameters in Model 1 based on average light intensity. As biomass decay rate is also dependent on temperature, μ_d has different values at different temperatures. Since the

current research does not focus on the relation between μ_d and temperature, values of μ_d at different temperatures are simply presented in Table 1. Figure 2 shows the comparison between Model 1 simulation results and experimental results.

Table 1: Parameters in average light intensity based Model 1 (*H. pluvialis* ZY-18)

Parameter	Value	Parameter	Value
k_q	0.151	$\mu_{d,28}$, L·hr^{-1}·g^{-1}	0.0096
k_s, μmol·m^{-2}·s^{-1}	300.0	k_{qw}	0.202
E_a, kJ·mol^{-1}	30.38	b	0.126
E_b, kJ·mol^{-1}	465.17	$w_{\max}$	3.80
A, hr^{-1}	3.35×10^{5}	k_{sw}, μmol·m^{-2}·s^{-1}	150.0
B, hr^{-1}	8.03×10^{79}	A_w, hr^{-1}	1.28×10^{14}
$\mu_{d,8}$, L·hr^{-1}·g^{-1}	0.0413	B_w, hr^{-1}	3.73×10^{42}
$\mu_{d,13}$, L·hr^{-1}·g^{-1}	0.0425	E_{aw}, kJ·mol^{-1}	73.69
$\mu_{d,18}$, L·hr^{-1}·g^{-1}	0.0287	E_{bw}, kJ·mol^{-1}	239.96
$\mu_{d,23}$, L·hr^{-1}·g^{-1}	0.0236	α, m^{2}·g^{-1}	0.050
k_l, m^{-1}	0.0		

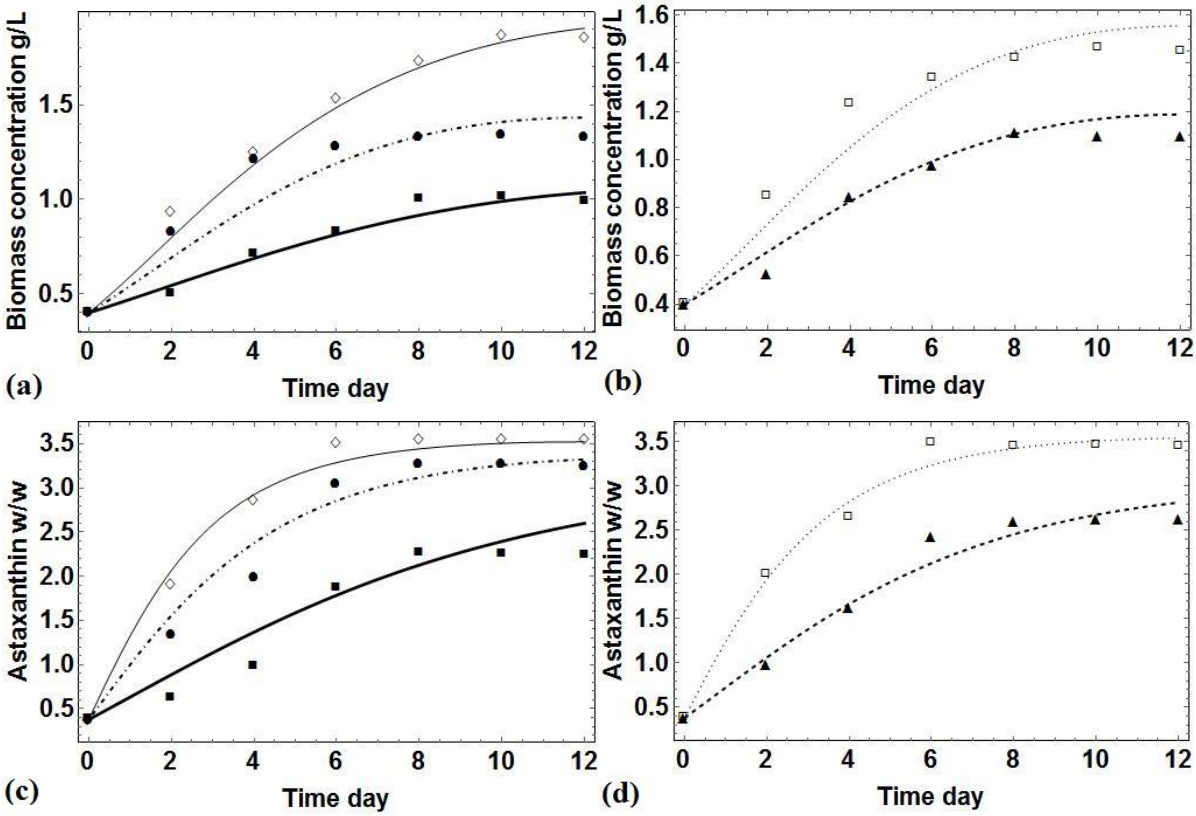

Figure 2: Comparison of experimental results and simulation results of average light intensity based Model 1 (*H. pluvialis* ZY-18). Thick solid line: simulation results at 8℃, dotted line: simulation results at 13℃, dot-dashed line: simulation results at 18℃, dashed line: 23℃, thin solid line: 28℃. Filled square: experimental results of 8℃, unfilled square: experimental results at 13℃, filled circle: 18℃, filled triangle: 23℃, unfilled diamond: 28℃.

From Figure 2, it can be seen that the model is capable of capturing accurately the trends of both biomass growth and astaxanthin accumulation. The comparison between Model 1 and Model 2 (average light intensity based) shows that they have very similar behaviour, which means that both can be selected for further work. By comparing the results of the average light intensity based model and the average growth rate based model, it is concluded that both simplification strategies show very similar behaviour and are close to the experimental data.

Therefore, these two strategies are both acceptable for future study.

It is notable that bubble scattering coefficient (k_l) is estimated to be zero in Table 1. Although previous research demonstrated that bubble scattering may play an important role causing light attenuation in a low biomass concentration culture [32], [50], its zero value calculated through the current parameter estimation procedure indicates that its effect on light attenuation is negligible compared to that of cell absorption in the current study. This conclusion is also consistent with recent studies which found that light attenuation is predominantly led by cell absorption instead of bubble scattering for cyanobacterial biohydrogen and C-phycocyanin production [37], [51].

3.2 Parameters in *H. pluvialis* NIES-144 models

For *H. pluvialis* NIES-144, both the suspended reactor and the attached reactor were used in this work. Temperature was fixed at 25℃. The Arrhenius equation is reduced to a constant in both models, and represented as μ_X and μ_w, for biomass growth and astaxanthin production, respectively. Table 2 shows the parameters in Model 1 based on average light intensity for the simulation of the suspended reactor. Figure 3 shows the comparison of Model 1 with the experimental results. It is also found that both the average light intensity based model and the average growth rate based model have very similar behaviour.

Table 2: Parameters in average light intensity based Model 1 (*H. pluvialis* NIES-144)

Parameter	Value	Parameter	Value

k_q	0.302	μ_d, L·hr^{-1}·g^{-1}	0.0414
k_s, μmol·m^{-2}·s^{-1}	300.0	k_{qw}	0.0505
μ_X, hr^{-1}	0.697	b	2.96×10^4
μ_w, hr^{-1}	1.02×10^{-4}	$w_{\max}$	3.80
α, m^2·g^{-1}	0.050	k_{sw}, μmol·m^{-2}·s^{-1}	150.0
k_l, m^{-1}	0.0		

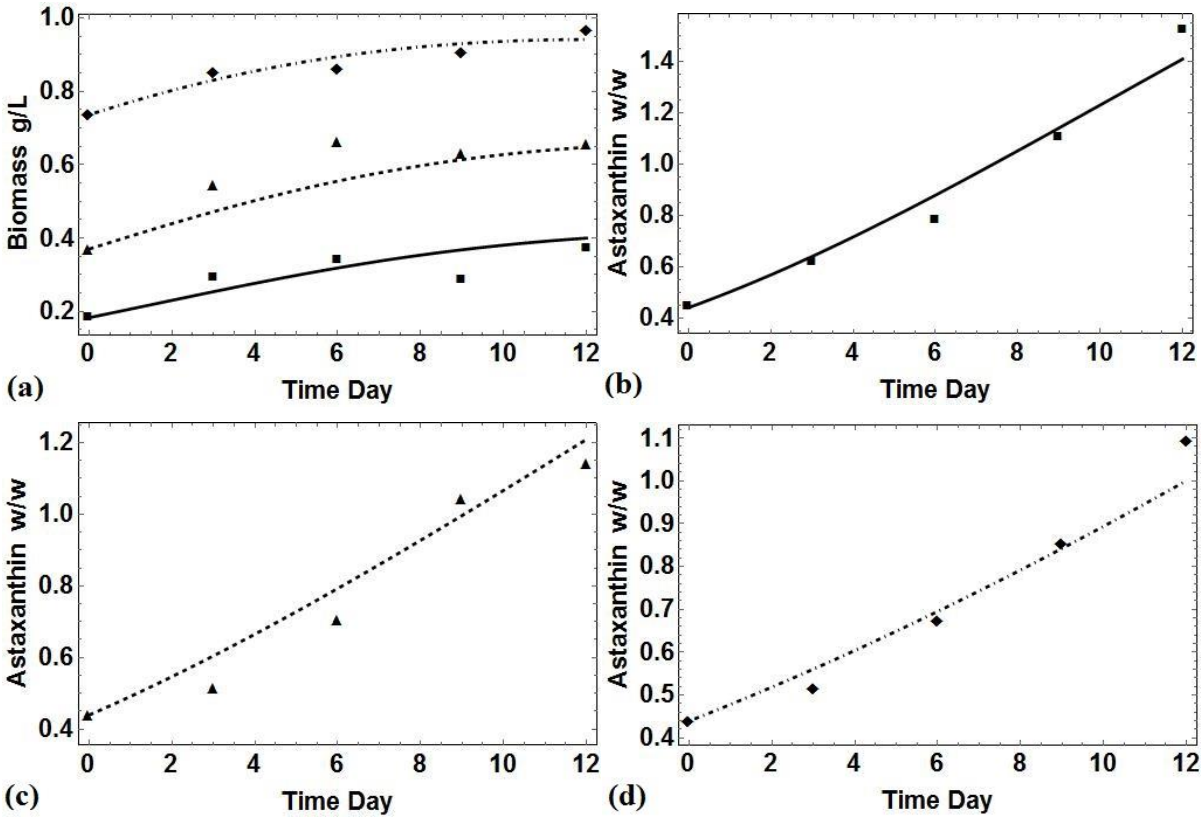

Figure 3: Simulation results of average light intensity based Model 1 (*H. pluvialis* NIES-144). (a): biomass concentration at different days, (b)-(d): astaxanthin accumulation during the process. Solid line and square: initial biomass concentration is 0.183 g·L^{-1}, dashed line and triangle: initial biomass concentration 0.370 g·L^{-1}, dot-dashed line and diamond: initial biomass concentration is 0.736 g·L^{-1}. Lines are simulation results and points are experimental

397 measurements.

398

399 However, Model 2 fails to capture accurately the *H. pluvialis* NIES-144 photo-fermentation
400 process in the suspended reactor because the growth phase was significantly extended. As the
401 difference between Model 1 and Model 2 is whether nitrogen-deficiency can stimulate the
402 biomass growth, the current research finds that in a suspended reactor, nitrogen-deficiency
403 does not remarkably increase the biomass growth rate of algae, and actually leads to a
404 decreasing biomass growth rate right from the beginning of the process.

405

406 A completely different conclusion is found when simulating the *H. pluvialis* NIES-144
407 photo-fermentation process in the attached reactor. Table 3 shows the parameters in Model 2
408 based on average light intensity for the simulation of the attached reactor. Figure 4 shows the
409 comparison of Model 2 simulation results and experimental measurements. From Figure 4, it
410 is found that the experimentally observed tendency is accurately captured by Model 2.
411 However, Model 1 does not fit the experimental data very well, as its simulation results
412 apparently reduce the algal growth period. Hence, it is concluded that in the attached reactor
413 nitrogen-deficiency does enhance biomass growth rate at the beginning and then limits cell
414 growth at the end. Both the average light intensity based model, and the average growth rate
415 based model, show very similar results as mentioned earlier.

416

417 Table 3: Parameters in average light intensity based Model 2 (*H. pluvialis* NIES-144)

Parameter	Value	Parameter	Value

k_q	0.165	μ_d, L·hr^{-1}·g^{-1}	8.54×10^{-4}
k_s, μmol·m^{-2}·s^{-1}	20.0	k_{qw}	0.47
μ_X, hr^{-1}	0.783	b	1.30
μ_w, hr^{-1}	0.434	$w_{\max}$	7.0
β, m^2·g^{-1}	0.0547	k_{sw}, μmol·m^{-2}·s^{-1}	300.0

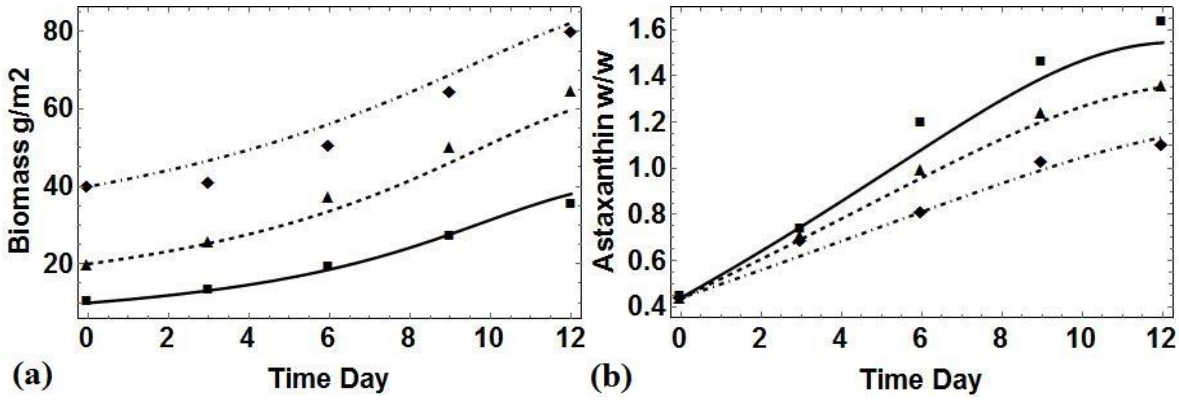

Figure 4: Simulation results of average light intensity based Model 2 (*H. pluvialis* NIES-144). Solid line and square: initial biomass concentration is 10.0 g·m^{-2}, dashed line and triangle: initial biomass concentration 20.0 g·m^{-2}, dot-dashed line and diamond: initial biomass concentration is 40.0 g·m^{-2}.

3.3 Model predictability

To identify the predictability of current models for different *H. pluvialis* strains astaxanthin production process, two additional experiments were carried out. The first experiment (Experiment 1) has the initial biomass concentration of 0.35 g L^{-1}, with incident light intensity of 150 μmol·m^{-2}·s^{-1} and temperature of 25℃. The strain used in this experiment is *H. pluvialis* NIES-144. The second experiment (Experiment 2) has the initial biomass

concentration of 0.3 g L^{-1}, with incident light intensity of 250 μmol·m^{-2}·s^{-1} and temperature of 28 ℃. The strain selected in the experiment is *H. pluvialis* ZY-18. Figure 5 shows the comparison between the current model simulation results and experimental data. From the figure, it can be concluded that the current models can accurately predict the dynamic performance of green algal astaxanthin production process with different operating conditions. Thus the model predictability is verified.

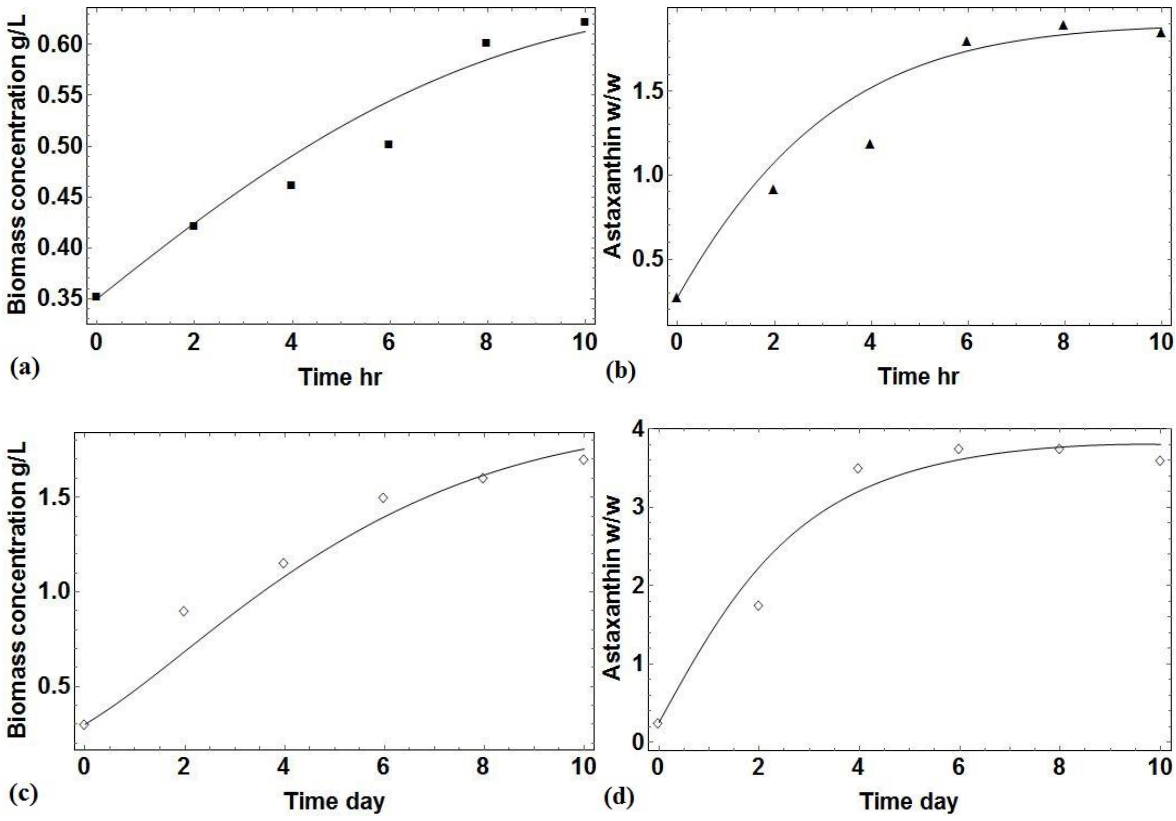

Figure 5: Comparison of experimental results and simulation results of average light intensity based Model 1. Thick solid line: simulation results, points: experimental data. (a) and (b): biomass concentration and astaxanthin content in Experiment 1, respectively. (c) and (d): biomass concentration and astaxanthin content in Experiment 2, respectively.

3.4 Temperature effects

Figure 6 presents the effects of temperature on both algal growth and astaxanthin production rate (activity), which are estimated based on Equation (16). From Figure 6, it can be seen that the optimal temperature for both algal growth and astaxanthin accumulation is 27℃ (300 K). Activities of enzymes for cell growth and bioproduct synthesis increase rapidly with the increasing temperature when it is lower than the optimal value, and then dramatically decrease if the temperature exceeds its optimal value. For example, algae almost stop growing once the temperature is higher than 31℃, with the production of astaxanthin also ceasing beyond this temperature. At a higher temperature (33℃), recent research found that a rapid cell decay phase with a significant reduction of astaxanthin content can be observed only two days after the beginning of the astaxanthin induction process [11]. The narrow range of suitable temperature values for algal growth and astaxanthin synthesis indicates that it is essential to control precisely the culture temperature in this bioprocess.

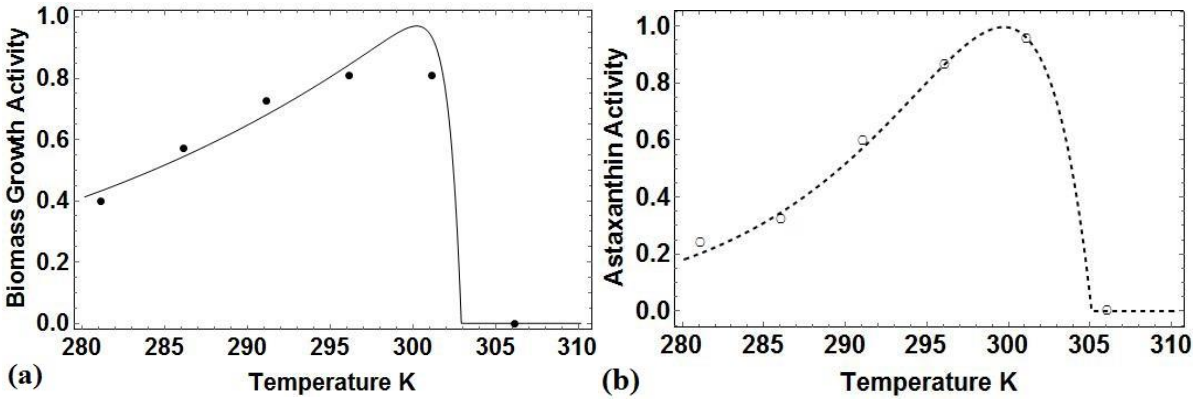

Figure 6: Effects of temperature on biomass growth and astaxanthin synthesis rate (activity). (a) effect of temperature on biomass growth rate; (b) effect of temperature on astaxanthin synthesis rate.

3.5 Light attenuation effects

In general, light attenuation is mainly caused by bubble reflection in low cell density cultures, and by algal absorption in high cell density cultures. Although in the current suspended reactor bubbles could be apparently observed, the simulation results show that bubble reflection for both *H. pluvialis* species is negligible as the term representing this factor (k_l) is estimated to be almost zero. Therefore, the primary factor causing light attenuation is algal absorption. To explore whether light attenuation is severe in the current suspended reactor, Figure 7 shows the local light intensity and cell growth rate at different biomass concentrations.

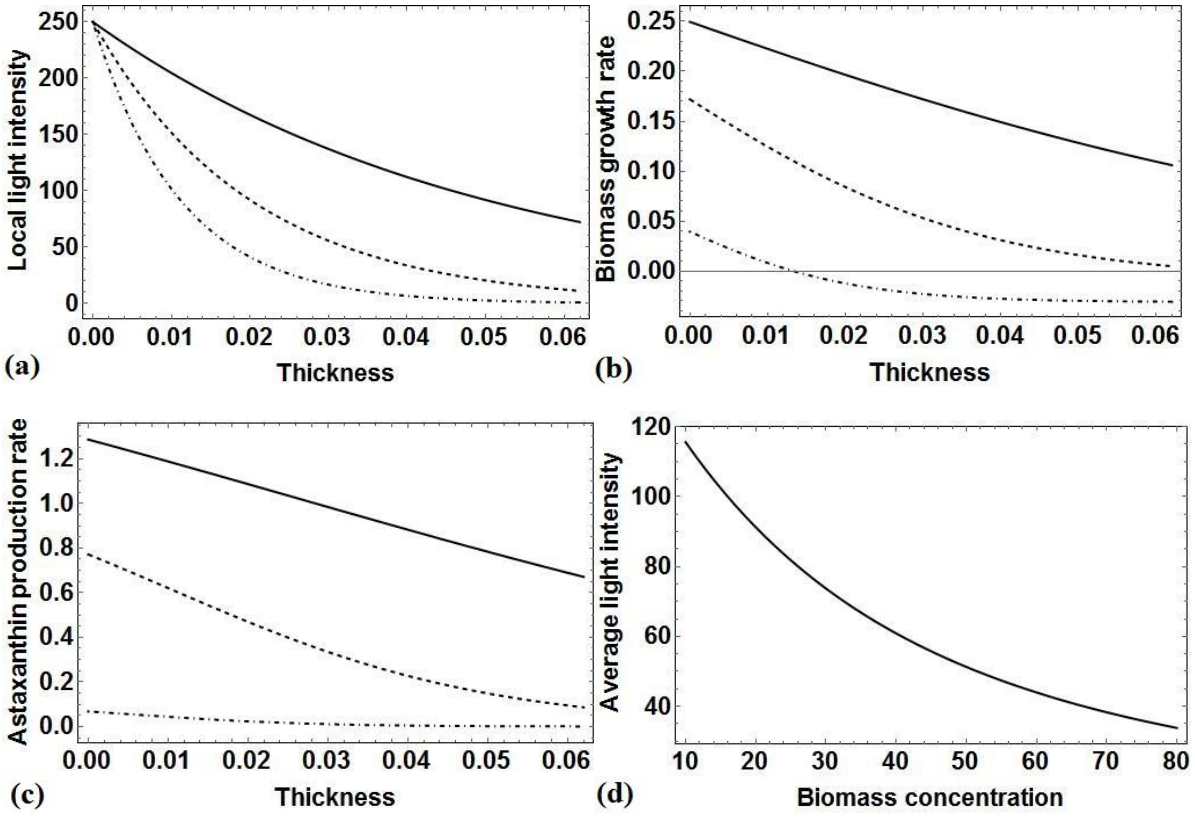

Figure 7: Light attenuation effects on biomass growth and astaxanthin accumulation. (a)-(c): Local light intensity ($\mu mol \cdot m^{-2} \cdot s^{-1}$), local biomass growth rate ($g \cdot L^{-1} \cdot hr^{-1}$) and local

477 astaxanthin accumulation rate ($g \cdot g^{-1} \cdot hr^{-1}$) of *H. pluvialis* ZY-18 at 28℃ in the suspended
478 reactor. The incident light intensity is 250$\mu mol \cdot m^{-2} \cdot s^{-1}$ and the reactor equivalent thickness is
479 0.062 m. The exposure surface corresponds to the front surface (x-axis 0.0 m). Solid line:
480 biomass concentration 0.4 $g \cdot L^{-1}$, dashed line: biomass concentration 1.0 $g \cdot L^{-1}$, dot-dashed line:
481 biomass concentration 1.8 $g \cdot L^{-1}$. (d): Average light intensity ($\mu mol \cdot m^{-2} \cdot s^{-1}$) at different biomass
482 concentration of *H. pluvialis* NIES-144 at 25℃ in the attached reactor. The incident light
483 intensity is 150$\mu mol \cdot m^{-2} \cdot s^{-1}$.
484
485 From Figure 7(a), it is found that light attenuation is always severe even at the initial
486 experimental period where biomass concentration is dilute (0.4 $g \cdot L^{-1}$). Local light intensity at
487 the back surface of the reactor is reduced by 71.1%. At a higher biomass concentration (1.0
488 $g \cdot L^{-1}$), cell absorption is more significant and local illumination is almost reduced to 10
489 $\mu mol \cdot m^{-2} \cdot s^{-1}$ at the back surface. More than half of the reactor volume is subjected to the severe
490 photo-limitation. Eventually, at the final cultivation period where cell density increases to 1.8
491 $g \cdot L^{-1}$, light cannot even pass through the whole volume of the current PBR, with most of the
492 reactor volume being in the dark zone.
493
494 Because of the light attenuation effects, local cell growth rate in the PBR almost decreases to
495 zero at the back surface when biomass concentration is 1.0 $g \cdot L^{-1}$ (Figure 7(b)). In the final
496 operation period, the algal growth rate is even lower than the algal decay rate in most of the
497 reactor volume, because the low illumination cannot facilitate cell photo-autotrophic growth.
498 Hence, biomass growth rate in the light zone is totally offset by its decay rate in the dark zone,

and the overall growth rate reduces to zero.

In terms of astaxanthin accumulation, two different factors contribute to the decrease of the astaxanthin accumulation rate. In the initial period, when cell density increases from 0.4 $g \cdot L^{-1}$ to 1.0 $g \cdot L^{-1}$, light attenuation is shown to be the primary factor limiting astaxanthin production. This is explained by the fact that the local astaxanthin accumulation rate in the reactor decreases with the decreasing local illumination along the light transmission direction (Fig. 7(c)), and astaxanthin content is still much lower (2.58%) than its maximum content (3.80%) [11]. However in the final operation period, as astaxanthin content is almost saturated (3.49% when biomass concentration is 1.8 $g \cdot L^{-1}$) the metabolic pathway of astaxanthin production is terminated. Hence, light attenuation is not important for astaxanthin production since the production rate is almost zero regardless of the local illumination intensity (Figure 7(c)).

In the case of the attached reactor, as there is no bubble pumping through the biofilm, light attenuation is purely induced by cell absorption. This is very different to what was found in the suspended reactor, with light attenuation in the attached reactor is significantly reduced. For example, the average light intensity in the attached reactor is 77.0% of the incident light intensity when biomass concentration is 10 $g \cdot m^{-2}$, while at this biomass concentration (0.18 $g \cdot L^{-1}$, equivalent to 10 $g \cdot m^{-2}$) the average light intensity in the current suspended reactor is only 48.5% of the incident light intensity. Therefore, the current attached reactor is found to enhance both biomass growth and astaxanthin accumulation rates due to its better light permeation.

However, average light intensity in the attached reactor also decreases rapidly with increasing biomass concentration (Figure 7(d)). The average light intensity is reduced to 50% of the incident light intensity when biomass concentration is 30 $g \cdot m^{-2}$, and to 20% of incident light intensity when biomass concentration reaches 80 $g \cdot m^{-2}$. Contrary to the case of the suspended reactor where cells are well mixed, cells in the attached reactor are fixed and those in the bottom of the biofilm always receive much less illumination compared to those on the top.

Because of the severe light attenuation caused by high biomass concentration, it is quite possible that cells in the bottom cannot receive enough light to stimulate the accumulation of astaxanthin. In fact, recent research [5] has found that in an attached reactor, similar to the currently considered reactor, cells located in the upper layer of the biofilm turn red while those in the bottom layer still remain green during the astaxanthin accumulation process. This observation proves the current simulation hypothesis that the severe light attenuation in an attached reactor may reduce astaxanthin production for the bottom cells.

Overall, in a suspended reactor, light attenuation is always significant and limits biomass growth. The accumulation of astaxanthin is initially limited by the low local light intensity due to light attenuation, but eventually it becomes independent of it as its content approaches to the maximum value. Although the attached reactor can provide a betters local light distribution and facilitate biomass growth, it can also prevent the accumulation of astaxanthin in the bottom layer algae, and the separation between red cells and green cells in a biofilm is also difficult to conduct in practice.

4 Conclusion

In the present study, two dynamic models have been constructed to simulate the growth of *H. pluvialis* and the associated astaxanthin production in a nitrogen-deprived culture, considering both attached and suspended photobioreactors.

To the best of our knowledge, this is the first ever attempt that the effects of light attenuation, temperature and nitrogen quota on cell growth and astaxanthin accumulation be included in unified models. By comparing the simulation results obtained with our experimental measurements, the accuracy of the current models is verified. Specifically, it is found that Model 1 is more accurate to simulate the astaxanthin accumulation process in a suspended reactor, while Model 2 is suitable for the simulation of this process in an attached reactor.

Using either an average light intensity or an average cell growth rate, to render the model one-dimensional, has been found to be a very accurate model simplification approach. Based on the current models proposed, the optimal temperature for both algal growth and astaxanthin accumulation has been determined.

Light attenuation in the suspended reactor is found to be mainly due to cell absorption, and primarily limits astaxanthin accumulation when astaxanthin concentration is much lower than its maximum value. When the astaxanthin content approaches to its maximum value, the effect of light attenuation on astaxanthin production becomes negligible.

Because of the reduced light attenuation in the attached reactor, biomass growth is much facilitated by this reactor type. However, a suspended reactor is still a better choice than an attached reactor for astaxanthin production, as in this reactor type most cells can be induced for astaxanthin accumulation.

In terms of future work, as the accumulation of astaxanthin may affect the cell absorption cross-section, the effect of its intracellular concentration on light attenuation will also be included in the current model to improve the model accuracy. In addition, as the reason why the effect of nitrogen-deficiency on cell growth is different between the two types of photobioreactors are still unclear, further metabolic kinetics studies will be addressed to clarify this observation.

Acknowledgment

Author D. Zhang gratefully acknowledges the support from his family. Author M. Wan, W. Wang, J. Huang and Y. Li are funded by National High Technology Research and Development Program of China (2015AA020602), National Key Technologies R&D Program (2011BAD23B04), National Basic Research Program of China (973 Program: 2011CB200903 & 2011CB200904), China Postdoctoral Science Foundation (2014T70400), the Fundamental Research Funds for the Central Universities (222201414024). Author E. A. del Rio-Chanona is funded by CONACyT scholarship No. 522530 from the Secretariat of Public Education and the Mexican government.

References

[1] E. Del R ó, F. G. Aci én, M. C. Garc á-Malea, J. Rivas, E. Molina-Grima, and M. G. Guerrero, "Efficient one-step production of astaxanthin by the microalga Haematococcus pluvialis in continuous culture.," *Biotechnol. Bioeng.*, vol. 91, no. 7, pp. 808–15, 2005.

[2] J. Fábregas, A. Otero, A. Maseda, and A. Domínguez, "Two-stage cultures for the production of Astaxanthin from Haematococcus pluvialis," *J. Biotechnol.*, vol. 89, no. 1, pp. 65–71, 2001.

[3] J. Wang, M. R. Sommerfeld, C. Lu, and Q. Hu, "Combined effect of initial biomass density and nitrogen concentration on growth and astaxanthin production of Haematococcus pluvialis (Chlorophyta) in outdoor cultivation," *Algae*, vol. 28, no. 2, pp. 193–202, 2013.

[4] M. Wan, D. Hou, Y. Li, J. Fan, J. Huang, S. Liang, W. Wang, R. Pan, J. Wang, and S. Li, "The effective photoinduction of Haematococcus pluvialis for accumulating astaxanthin with attached cultivation.," *Bioresour. Technol.*, vol. 163, pp. 26–32, 2014.

[5] W. Zhang, J. Wang, J. Wang, and T. Liu, "Attached cultivation of Haematococcus pluvialis for astaxanthin production.," *Bioresour. Technol.*, vol. 158, pp. 329–35, 2014.

[6] R. R. Ambati, S. M. Phang, S. Ravi, and R. G. Aswathanarayana, "Astaxanthin: sources, extraction, stability, biological activities and its commercial applications--a review.," *Mar. Drugs*, vol. 12, no. 1, pp. 128–52, 2014.

[7] a. . Domínguez-Bocanegra, I. Guerrero Legarreta, F. Martinez Jeronimo, and a Tomasini Campocosio, "Influence of environmental and nutritional factors in the production of astaxanthin from Haematococcus pluvialis," *Bioresour. Technol.*, vol. 92, no. 2, pp. 209–214, 2004.

[8] L. Fan, A. Vonshak, and S. Boussiba, "Effect of temperature and irradiance on growth of Haematococcus pluvialis," *J. Phycol.*, vol. 30, no. 0, pp. 829–833, 1994.

[9] L. Giannelli, H. Yamada, T. Katsuda, and H. Yamaji, "Effects of temperature on the astaxanthin productivity and light harvesting characteristics of the green alga Haematococcus pluvialis," *J. Biosci. Bioeng.*, vol. xx, no. xx, 2014.

[10] F. Grognard, A. R. Akhmetzhanov, and O. Bernard, "Optimal strategies for biomass productivity maximization in a photobioreactor using natural light," *Automatica*, vol. 50, no. 2, pp. 359–368, 2014.

[11] M. Wan, J. Zhang, D. Hou, J. Fan, Y. Li, J. Huang, and J. Wang, "The effect of temperature on cell growth and astaxanthin accumulation of Haematococcus pluvialis during a light-dark cyclic cultivation.," *Bioresour. Technol.*, vol. 167, pp. 276–83, 2014.

[12] M. C. García-Malea, C. Brindley, E. Del Río, F. G. Acién, J. M. Fernández, and E. Molina, "Modelling of growth and accumulation of carotenoids in Haematococcus pluvialis as a function of irradiance and nutrients supply," *Biochem. Eng. J.*, vol. 26, no. 2–3, pp. 107–114, 2005.

[13] M. C. García-Malea, F. G. Acién, E. Del Río, J. M. Fernández, M. C. Cerón, M. G. Guerrero, and E. Molina-Grima, "Production of astaxanthin by Haematococcus pluvialis: taking the one-step system outdoors.," *Biotechnol. Bioeng.*, vol. 102, no. 2, pp. 651–7, 2009.

[14] X. Zhang, X. Gong, and F. Chen, "Kinetic models for astaxanthin production by high cell density mixotrophic culture of the microalga Haematococcus pluvialis," *J. Ind. Microbiol. Biotechnol.*, vol. 23, no. 0, pp. 691–696, 1999.

[15] X.-W. Zhang, X. Gong, and F. Chen, "Dynamics and stability analysis of the growth and astaxanthin production system of Haematococcus pluvialis," *J. Ind. Microbiol. Biotechnol.*, vol. 23, no. 0, pp. 133–137, 1999.

[16] M. Lu, L. Ji, Y. Liu, P. Zhou, and L. Yu, "Kinetic Model for Optimal Feeding Strategy in Astaxanthin Production by Xanthophyllomyces dendrorhous.," *Chin. J. Biotechnol.*, vol. 24, no. 11, pp. 1937–1942, 2008.

[17] D. Zhang, P. Dechatiwongse, E. A. Del-Rio-Chanona, K. Hellgardt, G. C. Maitland, and V. S. Vassiliadis, "Analysis of the Cyanobacterial Hydrogen Photo-Production Process via Model Identification and Process Simulation," *Chem. Eng. Sci.*, vol. 128, pp. 130–146, 2015.

[18] I. Vatcheva, H. de Jong, O. Bernard, and N. J. I. Mars, "Experiment selection for the discrimination of semi-quantitative models of dynamical systems," *Artif. Intell.*, vol. 170, no. 4–5, pp. 472–506, 2006.

[19] Y. Li, M. Sommerfeld, F. Chen, and Q. Hu, "Consumption of oxygen by astaxanthin biosynthesis: a protective mechanism against oxidative stress in Haematococcus pluvialis (Chlorophyceae).," *J. Plant Physiol.*, vol. 165, no. 17, pp. 1783–97, 2008.

[20] D. Han, Y. Li, and Q. Hu, "Astaxanthin in microalgae: pathways, functions and biotechnological implications," *Algae*, vol. 28, no. 2, pp. 131–147, 2013.

[21] W. Gu, H. Li, P. Zhao, R. Yu, G. Pan, S. Gao, X. Xie, A. Huang, L. He, and G. Wang, "Quantitative proteomic analysis of thylakoid from two microalgae (Haematococcus

654 pluvialis and Dunaliella salina) reveals two different high light-responsive strategies.,"
655 *Sci. Rep.*, vol. 4, pp. 1–12, 2014.

656 [22] M. Kobayashi, T. Kakizono, K. Yamaguchi, and N. Nishio, "Growth and Astaxanthin
657 Formation of Haematococcus pluvialis in Heterotrophic and Mixotrophic Conditions,"
658 *J. Ferment. Bioeng.*, vol. 74, no. 1, pp. 17–20, 1992.

659 [23] J. Wang, D. Han, M. R. Sommerfeld, C. Lu, and Q. Hu, "Effect of initial biomass
660 density on growth and astaxanthin production of Haematococcus pluvialis in an
661 outdoor photobioreactor," *J. Appl. Phycol.*, vol. 25, no. 1, pp. 253–260, 2012.

662 [24] T. Goksan and I. Ak, "Vegetative growth of the green alga Haematococcus pluvialis
663 cultivated in different light-path lengths," *Asian J. Plant Sci.*, vol. 5, no. 3, pp. 455–
664 460, 2006.

665 [25] E. Imamoglu, M. C. Dalay, and F. V. Sukan, "Influences of different stress media and
666 high light intensities on accumulation of astaxanthin in the green alga Haematococcus
667 pluvialis.," *N. Biotechnol.*, vol. 26, no. 3–4, pp. 199–204, 2009.

668 [26] S. Aiba, "Growth Kinetics of Photosynthetic Microorganisms.," *Adv. Biochem. Eng.*,
669 vol. 23, no. 0, pp. 85–156, 1982.

670 [27] B. W. Kim, H. N. Chang, I. K. Kim, and K. S. Lee, "Growth kinetics of the
671 photosynthetic bacterium Chlorobium thiosulfatophilum in a fed-batch reactor.,"
672 *Biotechnol. Bioeng.*, vol. 40, no. 5, pp. 583–592, 1992.

673 [28] H. Berberoglu, J. Yin, and L. Pilon, "Light transfer in bubble sparged photobioreactors
674 for H2 production and CO2 mitigation," *Int. J. Hydrogen Energy*, vol. 32, no. 13, pp.
675 2273–2285, 2007.

676 [29] E. Molina Grima, F. Garcia Camacho, J. A. Sanchez Perez, J. M. Fernandez Sevilla, F.
677 G. Acien Fernandez, and A. Contreras Gomez, "A mathematical model of microalgal
678 growth in light-limited chemostat culture," *J. Chem. Technol. Biotechnol.*, vol. 61, no.
679 2, pp. 167–173, 1994.

680 [30] Z. Cui and L. S. Fan, "Turbulence energy distributions in bubbling gas-liquid and
681 gas-liquid-solid flow systems," *Chem. Eng. Sci.*, vol. 59, no. 8–9, pp. 1755–1766,
682 2004.

683 [31] R. Kandilian, T.-C. Tsao, and L. Pilon, "Control of incident irradiance on a batch
684 operated flat-plate photobioreactor," *Chem. Eng. Sci.*, vol. 119, pp. 99–108, 2014.

685 [32] D. Zhang, P. Dechatiwongse, and K. Hellgardt, "Modelling light transmission,
686 cyanobacterial growth kinetics and fluid dynamics in a laboratory scale multiphase

687 photo-bioreactor for biological hydrogen production," *Algal Res.*, vol. 8, no. 0, pp. 99–
688 107, 2015.

689 [33] F. G. Acie, J. A. Sa, and E. M. Grima, "A Model for Light Distribution and Average
690 Solar Irradiance Inside Outdoor Tubular Photobioreactors for the Microalgal Mass
691 Culture," *Biotechnol. Bioeng.*, vol. 55, no. 5, pp. 701–714, 1997.

692 [34] E. M. Grima, J. A. S. Prez, F. G. Camacho, J. M. F. Sevilla, and F. G. A. Fernandez,
693 "Productivity analysis of outdoor chemostat culture in tubular air-lift photobioreactors,"
694 *J. Appl. Phycol.*, vol. 8, no. 0, pp. 369–380, 1996.

695 [35] D. Zhang, N. Xiao, K. T. Mahbubani, E. A. del Rio-Chanona, N. K. H. Slater, and V. S.
696 Vassiliadis, "Bioprocess modelling of biohydrogen production by Rhodopseudomonas
697 palustris: Model development and effects of operating conditions on hydrogen yield
698 and glycerol conversion efficiency," *Chem. Eng. Sci.*, vol. 130, pp. 68–78, 2015.

699 [36] E. A. del Rio-Chanona, P. Dechatiwongse, D. Zhang, G. C. Maitland, K. Hellgardt, H.
700 Arellano-Garcia, and V. S. Vassiliadis, "Optimal Operation Strategy for Biohydrogen
701 Production," *Ind. Eng. Chem. Res.*, vol. 54, no. 24, pp. 6334–6343, 2015.

702 [37] E. A. del Rio-Chanona, D. Zhang, Y. Xie, E. Manirafasha, and K. Jing, "Dynamic
703 Simulation and Optimization for Arthrospira platensis Growth and C-Phycocyanin
704 Production," *Ind. Eng. Chem. Res.*, p. 151021162033007, 2015.

705 [38] C. Barranguet, S. A. M. va. Beusekom, B. Veuger, T. R. Neu, E. M. M. Manders, J. J.
706 Sinke, and W. Admiraal, "Study undisturbed autotrophic biofilms: still a technical
707 challenge.," *Aquat. Microb. Ecol.*, vol. 34, no. 0, pp. 1–9, 2004.

708 [39] R. Chen, Y.-K. Pu, Q. Liao, X. Zhu, and Y.-Z. Wang, "A simulation on PSB biofilm
709 formation with considering cell inactivation," *Int. J. Hydrogen Energy*, vol. 38, no. 35,
710 pp. 15670–15679, 2013.

711 [40] P. J. Schnurr, G. S. Espie, and D. G. Allen, "The effect of light direction and
712 suspended cell concentrations on algal biofilm growth rates.," *Appl. Microbiol.*
713 *Biotechnol.*, vol. 98, no. 20, pp. 8553–62, 2014.

714 [41] M. C. Garc á-Malea, F. G. Aci én, J. M. Fern ández, M. C. Cer ón, and E. Molina,
715 "Continuous production of green cells of Haematococcus pluvialis: Modeling of the
716 irradiance effect," *Enzyme Microb. Technol.*, vol. 38, no. 7, pp. 981–989, 2006.

717 [42] D. Zhang, P. Dechatiwongse, E. A. del Rio-Chanona, G. C. Maitland, K. Hellgardt,
718 and V. S. Vassiliadis, "Modelling of light and temperature influences on
719 cyanobacterial growth and biohydrogen production," *Algal Res.*, vol. 9, pp. 263–274,
720 2015.

[43] G. Alagappan and R. M. Cowan, “Effect of Temperature and Dissolved Oxygen on the Growth Kinetics of Pseudomonas Putida F1 Growing on Benzene and Toluene.,” *Chemosphere*, vol. 54, no. 8, pp. 1255–65, 2004.

[44] V. S. Brauer, M. Stomp, C. Rosso, S. a M. van Beusekom, B. Emmerich, L. J. Stal, and J. Huisman, “Low temperature delays timing and enhances the cost of nitrogen fixation in the unicellular cyanobacterium Cyanothece.,” *ISME J.*, vol. 7, no. 11, pp. 2105–15, 2013.

[45] J. V. C. Vargas, a. B. Mariano, D. O. Corrêa, and J. C. Ordonez, “The microalgae derived hydrogen process in compact photobioreactors,” *Int. J. Hydrogen Energy*, vol. 39, no. 18, pp. 9588–9598, 2014.

[46] L. Brugnano, F. Mazzia, D. Trigiante, T. E. Simos, G. Psihoyios, and C. Tsitouras, “The Role of the Precise Definition of Stiffness in Designing Codes for the Solution of ODEs.,” in *AIP Conference Proceedings*, 2009, pp. 731–734.

[47] E. Hairer and G. Wanner, *Solving Ordinary Differential Equations II*, 2nd ed., vol. 14. Berlin, Heidelberg: Springer Berlin Heidelberg, 1996.

[48] W. E. Hart, C. Laird, J.-P. Watson, and D. L. Woodruff, *Pyomo – Optimization Modeling in Python*, vol. 67. Boston, MA: Springer US, 2012.

[49] A. Wächter and L. T. Biegler, *On the implementation of an interior-point filter line-search algorithm for large-scale nonlinear programming*, vol. 106, no. 1. 2005.

[50] D. Zhang, E. A. D.-R. Chanona, V. S. Vassiliadis, and B. Tamburic, “Analysis of green algal growth via dynamic model simulation and process optimization,” *Biotechnol. Bioeng.*, vol. 112, no. 10, pp. 2025–2039, 2015.

[51] D. Zhang, P. Dechatiwongse, E. A. del Rio-Chanona, G. C. Maitland, K. Hellgardt, and V. S. Vassiliadis, “Dynamic modelling of high biomass density cultivation and biohydrogen production in different scales of flat plate photobioreactors,” *Biotechnol. Bioeng.*, vol. 112, no. 12, pp. 2429–2438, 2015.